Journal of Photochemistry and Photobiology A: Chemistry 347 (2017) 67–77

Contents lists available at ScienceDirect

Journal of Photochemistry and Photobiology A: Chemistry

journal homepage: www.elsevier.com/locate/jphotochem

Invited paper

Highly luminescent anthracene sulfides. Synthesis, experimental and DFT study of their optical properties and interaction with electron deficient nitroaromatic compounds

Claudia M. Hegguilustoy, Rosana S. Montani, Pablo G. Del Rosso, Maria J. Romagnoli, Raúl O. Garay*

INQUISUR, Departamento de Química, Universidad Nacional del Sur (UNS)-CONICET, Av. Alem 1253, 8000 Bahía Blanca, Argentina

ARTICLE INFO

Article history:
Received 28 May 2017
Accepted 7 July 2017
Available online 20 July 2017

Keywords:
Polysulfurated
Anthracene
Pyrene
Optical properties
TDDFT
Photooxidation
Chemosensor

ABSTRACT

We report on the synthesis, thermal and photooxidative behavior and optical properties of a series alkyl and aryl sulfides with anthracene cores. All anthracene sulfides studied here were highly fluorescent. Their optical behavior was compared with that of related pyrene bisulfide and tetrasulfides. All sulfides are crystalline compounds and show good chemical stability in condensed phase. In solution, the pyrene derivatives are very stable but the anthracene derivatives suffer a slow photooxidation process under air and ambient light. While the bisulfides of anthracene and pyrene have very different spectroscopic behavior, the tetrasubstituted anthracene and pyrene sulfides exhibit quite a few similarities. Thus, the chromophoric core of the compounds consists of the aromatic core and the sulfur or oxygen atoms, so the variation from alkyl to aryl substituents does not alter the profiles of the absorption and emission spectra. All they show intense fluorescence, but sulfides bearing SCH_2 or OCH_2 groups display higher fluorescence efficiencies than the ones with aryl substituents. In addition, their quenching efficiencies with nitroaromatic compounds of both series are dominated by steric hindrance rather than by electronic factors. Bathochromic shifts in the absorption spectra are well reproduced by TDDFT. Moreover, calculations indicate that the lower energy excitations are of non-ionic type in agreement with experimental results which showed that both absorption and emission spectra are devoid of noticeable solvatochromic effects.

1. Introduction

Aryl sulfides are notable building blocks for organic materials whose valuable properties were initially expressed in a polymeric structure, poly-*p*-phenylene sulfide, PPS, which became one of the most important high temperature thermoplastic polymers. Upon oxidation, PPS was also one of the first conductive polymers to be studied [1]. Later, aryl sulfides were included in a variety of molecular architectures such as oligomers [2,3], discotic liquid crystals [4,5], asterisks (a kind of star oligomers) [6], and dendrimers [7]. The interest in polysulfurated arenes springs from the interplay between the extended pi system and sulfur atoms with moderate electronegativity and d orbitals that originate electrophores with dual character, that is, they are able to stabilize either positive or negative charges. Thus, hexakis(arylthio) benzenes have been studied as ligands in analogues of biological electron transfer clusters [8], the electrical conductivities of tetrakis(alkylthio) bisphthalocyanines [9] and radical cation salts of tetrakis(alkylthio)pyrenes [10,11] have been assessed, the redox and electrochromic properties of coronene asterisks [12] and polysulfurated pyrene-cored dendrimers [7] were analyzed and the organic field-effect transistors properties of bis(methylthio) tetracenes [13] have also been tested.

By contrast, the photophysical properties of sulfurated arenes have received less attention than electronic ones. Recently, it was reported that persulfurated benzenes show very intense phosphorescence in conformationally restricted environments [14] that was used to develop a sensing system responsive to magnesium and fluoride [15]. But on the whole, the photophysical properties of polysulfurated arenes have remained rather unexplored since it was initially observed that persulfurated arenes with benzene [14] or corannulene cores [16] display no appreciable emission in solution. However, a few studies reported that polysulfurated pyrenes exhibit fluorescence in solution [7,17] while the

* Corresponding author.
E-mail address: rgaray@criba.edu.ar (R.O. Garay).

http://dx.doi.org/10.1016/j.jphotochem.2017.07.011
1010-6030/

performance of bis(alkylthio)- and bis(arylthio)anthracenes in electroluminescent devices [18] was measured. In the latter case, it was reported that quantum yields for the emission of the anthracene 9,10-bissulfides were quite low. Indeed, the low emission efficiencies displayed by some disubstituted anthracene derivatives have been often attributed to intersystem crossing [19,20]. It is difficult however to establish an emission pattern for anthracene derivatives. Thus, the quantum yields of 9,10-dimethoxyanthracene approach unity, 9-chloroanthracene shows no emission but the 9,10-dichloride does while both 9,10-dibromo- [20] and 9,10-bis(dimethylamino)anthracene [21] display very low quantum yields. Moreover, 1,5-, 2,6- and 9,10 distyrylanthracenes are luminescent organic semiconductors [22] while a 2,6,9,10-tetra (*p*-substituted-styryl)anthracene derivative shows very weak emission in THF solution [23].

Currently, we are interested in the use of aromatic fluorophores as the active elements of sensing materials either in polymeric assemblies or discrete molecules. In particular, we found that a fluorescent diphenylanthrylene-based polymer showed significant efficiency in chemosensing nitroaromatics [24]. We also noted during a reactivity study involving some anthracene tetrasulfides as products [25] that their chloroform solutions appeared highly fluorescent. So, they could be foreseen as very interesting organic semiconductors if their luminescent properties indeed parallel their excellent electronic properties. Therefore we undertook an investigation of their spectroscopic properties. To this end, the effect of additional phenylthio or alkoxy groups at the 2,6 positions of the structure of the weakly emitting 9,10-bis(phenylthio) anthracene **1** as well as the effect of replacing the phenylthio groups by alkylthio groups on the photophysical properties was studied (Scheme 1). Additionally, their optical behavior was compared with that of related bis(phenylthio)-, tetrakis(phenylthio)- and tetrakis(alkylthio)pyrene. The thermal properties, photooxidative behavior and fluorescence quenching by nitrobenzene and 3,4,6-trinitrotoluene of this series of highly fluorescent anthracene and pyrene sulfides are also reported. Conclusions

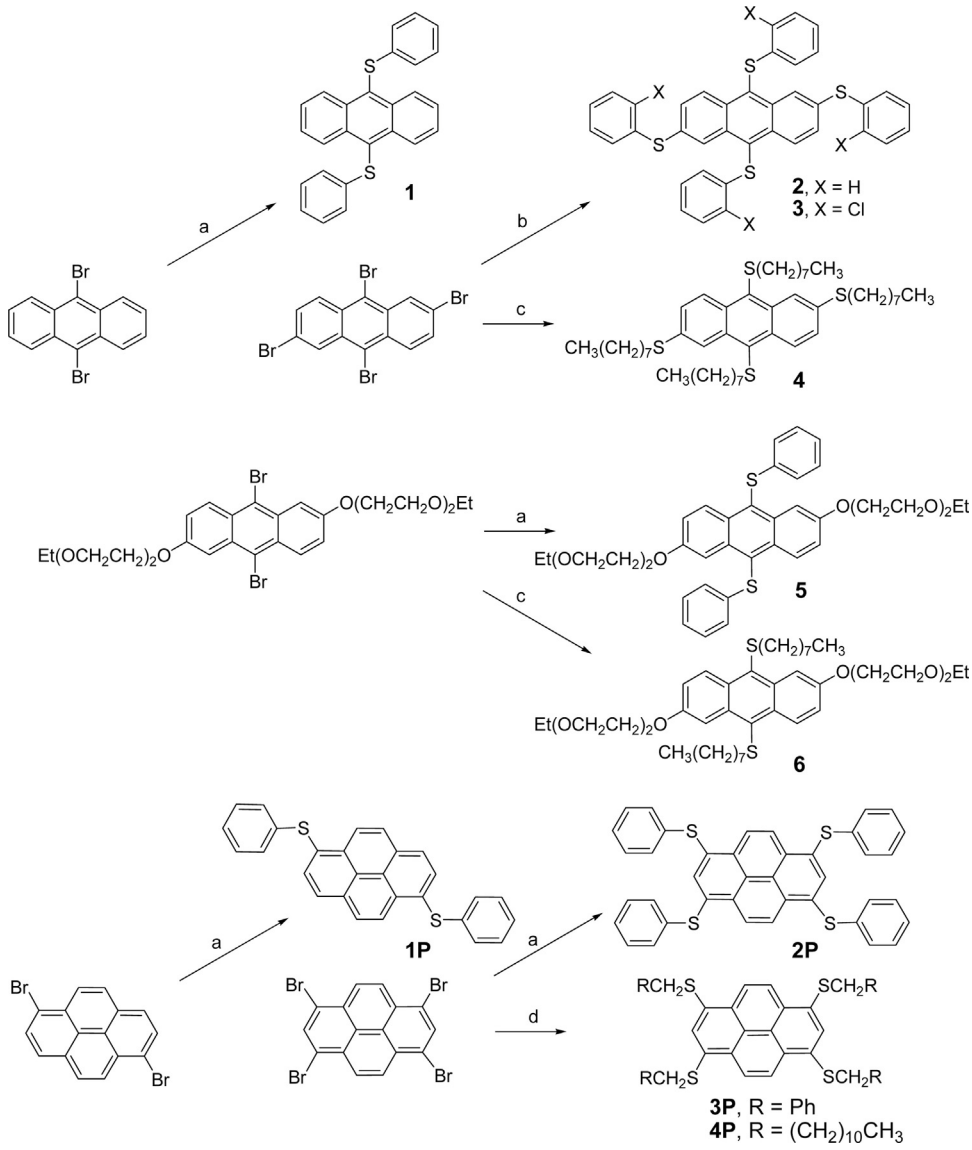

Scheme 1. Synthesis of the sulfide derivatives. Reactants and conditions: a) PhSH/Na/EtOH, vacuum, DMI/40 °C; b) *o*-XPhSH/Na/EtOH, vacuum, DMI/40 °C. c) $C_8H_{17}SH$/NaH/DMI/80 °C; d) RSH/NaH/DMF.

from experimental findings were discussed with the assistance of quantum chemistry calculations of the electronic structure (DFT) and absorption transitions (TD-DFT) of the polysulfides.

2. Experimental

2.1. Materials, general methods and analytical equipment

Reagents and solvents were purchased from Aldrich and used without further purification unless otherwise specified. Melting points are not corrected. ^{1}H NMR (300 MHz) and ^{13}C NMR (75 MHz) spectra were recorded on a Bruker AVANCE III spectrometer at 25 °C. Mass spectra were obtained with a GC/MS instrument (HP5-MS capillary column, 30 m × 0.25 mm × 0.25 μm) equipped with a 5972 mass selective detector operating at 70 eV (EI). Elemental analyses (C, H) were performed on an EXETER CE-440 instrument. Thermal analysis was carried out on a TA Q20 instrument under nitrogen flow at a scan rate of 10 °C/min. The thermal behavior was also analyzed by polarizing optical microscopy (POM) using an optical polarizing microscope (Leitz, Model Ortolux) equipped with a hot stage (Mettler). UV/vis spectra were obtained from a UV–vis GBC Cindra 20 spectrometer. The absorption measurements were done on dilute samples (less than 0.01 g/ml). The molar extinction coefficients (ε) were obtained from the slope of the plot of the absorption with six solutions of different concentrations *vs.* the concentration (correlation values ≥ 0.99). Fluorescence studies were conducted using a SML model 4800 spectrofluorometer at 25 °C. The emission measurements were carried out on dilute samples (less than 0.02 mg/ml) using a quartz cuvette with a path length of 1 cm and keeping the optical densities below 0.1. Fluorescence quantum yields of compound in THF solution were determined relative to equiabsorbing solutions of quinine sulphate (Φ_F = 0.546 in 0.5 M sulphuric acid) either in air equilibrated solutions or in nitrogen deaerated solutions.

2.2. Computational details

All calculations were performed with the ORCA program package [26]. Pre- and post-processing operations were performed by using the graphical interface Gabedit [27]. To reduce the computational expenses, the flexible side chains in derivatives of anthracene and pyrene were replaced by methyl groups. It has been shown that the effect of side chains on steady state optical properties is negligible [28,29]. Ground-state geometry optimizations used the B3LYP functional, the def2-TZVP(-f) basis set [30], a conductor-like screening model (COSMO) correction [31,32] for solvation effects and Grimme's dispersion energy term (D3) [33]. The COSMO term used the predefined parameters appropriate to THF. The vibrational spectrum was checked to ensure that no imaginary frequency was present. Thus the analytical determination of the Hessian matrix was made consistently using the same methodology as in the previous step. The excited state calculations were done at the optimized ground-state geometries, hence they correspond to vertical transitions. The absorption transitions were calculated on the basis of the time-dependent density functional theory (TD-DFT) within the TDA approximation [34] employing the B3LYP and the BHLYP hybrid functionals and the def2-TZVP(-f) basis set. All two-electron integral transformations were carried out applying the RI approximation [35] with auxiliary basis set [36].

3. Results and discussion

3.1. Synthesis

The bromides used as synthetic precursors for the corresponding sulfides were obtained by brominating the aromatic hydrocarbons (Scheme 1). Mild synthetic conditions were used to prepare the bis- and tetrakis(arylthio) derivatives by nucleophilic polysubstitution of the corresponding bromides using an excess sodium phenylthiolate in DMI at 40 °C for extended periods of time. This procedure is chemoselective and useful in the case of **3** since at that mild temperature the sodium 2-chlorobenzenethiolate self-attack does not occur [24]. The tetrakis(alkylthio) derivatives were synthesized using sodium alkylthiolate in DMI or DMF. Synthetic details are included in the Supporting information Section. All compounds are soluble in common organic solvents, e.g., toluene, benzene, $CHCl_3$ and THF, though solubility usually increases with the number of substituents and the replacement of aryl by alkyl or ethyleneoxy substituents. Full structural characterization of two of the anthracene sulfides studied here had been reported before, namely **1,** that was prepared by a different synthetic route than the one implemented for this work [25] and **3** which was previously reported by us [24].

Table 1
Thermal and photophysical properties of disulfides and tetrasulfides.

Cpd[a]	Tm[b]			Absorption		Emision			
	HC	CC	SC	$\lambda_{max(\varepsilon max)}$[c]		λ_{max}[d]	SS[e]	Φ_F[f]	Φ_F[g]
A	–	–	–	324, 341, 358, **377**	(0.83)	380, 402, 496	209		–
1	217	149	68	375(sh), 396, **416**	(1.04)	458	2204	0.02	0.02
2	208	133	75	396, **434**, 448	(0.56)	483	1568	0.24	0.26
3	234	160	74	385, **426**, 448	(1.83)	482	1538	0.30	0.63
4	86	67	19	395, 433, **447**	(0.88)	482	1538	0.49	0.59
5	72	42	30	397(sh), 416, **440**	(1.00)	480	1893	0.52	0.89
6	75	63	12	389(sh), 408, **433**	(0.92)	473	1953	0.70	0.98
P	–	–	–	295, 306, 320, **336**	(5.10)	**373**, 379, 384	2952		
1P	216	164	52	367, **384**	(3.40)	**412**, 431	1769	0.16	0.31
2P	227	197	30	414, **435**	(3.70)	**453**, 474 (sh)	864	0.28	0.32
3P	178	116	61	413(sh), **429**	(5.00)	**449**, 471 (sh)	1066	0.68	0.92
4P	108	98	10	409(sh), **427**	(2.10)	**446**, 472	998	0.48	0.68

[a] **A** = anthracene.
[b] Melting transition temperature (°C) determined by DSC at scan rates of 5 °C/min. HC = heating cycle, CC = cooling cycle, SC = super cooling.
[c] Absorption maxima measured in dilute THF solutions (Extinction coefficients of mayor peak of the low energy bands, in 10^4 mol^{-1} cm^{-1} L). Bold data indicate the major peaks, in nm.
[d] Emission maxima measured in dilute THF solutions, in nm.
[e] Stokes shifts in dilute THF solutions and on films ($\lambda_{max,em}$- $\lambda_{max,abs}$, in cm^{-1}).
[f] Fluorescence quantum yields measured in air equilibrated THF solutions.
[g] Fluorescence quantum yields measured in deaerated THF solutions.

We had also reported preliminary characterization data and conditions to obtain **2** and **5** but they were not adequately purified and characterized. Curiously, the structurally simple **1P** had not been yet synthetized and for the pyrene **4P** only the melting point had been reported in the literature [9].

3.2. Thermal and photooxidative behavior

All sulfides are crystalline compounds according to evidence from DSC and POM experiments. The DSC results indicate that they can be repeatedly cycled to temperatures above their melting points in nitrogen atmosphere. Their DSC traces registered from −20 °C up to 260 °C showed only distinct melting and crystallization transitions while no glass transitions were observed; see Fig. S1 and Table 1. All of them showed only one melting transition in the second heating cycle, strong supercooling in the cooling cycle and no sign of the presence of a liquid crystalline phase either in the heating or the cooling cycles. Their non-mesomorphic nature was confirmed by POM visual observations in thin films placed between cross polarizers; only generic colorful crystal textures could be observed after cooling from the isotropic liquid state. As expected, the compounds with long flexible chains showed low melting transitions, i.e., below 100 °C, while the derivatives with aryl sulfide groups have higher melting transitions, ca. 200 °C, stronger supercooling and, on occasions, several very close melting and crystallization transitions which could be related to the presence of multiple polymorphs originated by the conformational freedom of the arylsulfides groups. For instance, **3** showed in the first heating cycle a melting transition at 229 °C coupled with a cold crystallization at 233 °C to finally melt at 245 °C, while in the second heating cycle only a transition at 234 °C to a metastable polymorph was detected (Fig. S2). Simple space-filling considerations indicate that the aryl groups linked by a sulfur atom with a C—S—C angle of ∼109° cannot lie in the same plane as the central aromatic core. These substituent groups must instead adopt conformations above or below such plane. Indeed, the DFT modeling of the geometry of the sulfides presented in the Section 3.4 supports this conception, see Fig. 4.

These sulfides show good chemical stability in condensed phase. Thus, their microcrystalline powers can stay months in open atmosphere exposed to light and air. In solution, the pyrene derivatives are also very stable but the anthracene derivatives degrade slowly under ambient conditions. Thus, a perceptible darkening occurred after a day or two when yellow-greenish chloroform solutions ($\sim 1 \times 10^{-3}$ M) of the sulfides compounds were kept under both air and ambient light.

Indeed, the solution ^{1}H NMR spectra of **1** in $CDCl_3$ showed new aromatic signals at 8.33 ppm and 7.81 ppm whose intensity grew with time, which can be assigned to anthraquinone, while no additional signals above 9 ppm could be observed (Fig. 1a). Although no attempts to isolate the oxidation products were made, the GC–MS analysis of a solution of **1** in $CDCl_3$ aged for 3 days showed the disulfide **1**, anthraquinone and PhSSPh as the predominant peaks in the GC–MS trace. We also found new signals at 8.09 ppm and 7.98 ppm in the spectrum of **2** after its recrystallization from toluene at 110 °C under air and ambient light (Fig. 1b), these signals could be tentatively assigned to aromatic protons of the 2,6-bis(benzylthio)anthraquinone. This rather clean photo-oxidative reactivity pattern matches the one observed in higher acenes and some of their disulfide derivatives [37]. The extension of the proposed mechanism to our systems suggests that the path towards decomposition for the 9,10-thioanthracene sulfides here observed consists first in the formation of $^1O_2$ adducts in the 9,10 position and the subsequent concerted extrusion of the disulfide from the endoperoxide intermediate to render the corresponding anthraquinone and the dialkyl or diaryl disulfide.

The photooxidation reaction was also monitored for the other anthracene sulfides. All of them show signals whose intensity increased with time in their ^{1}H NMR spectra which can be attributed to aromatic oxidation products. The alkylthio derivatives were found to be more stable than the phenylthio ones while the 2,6-dialkoxy derivatives were the more stable ones though they showed a more complex reaction pattern than **1** or **2**. Thus, the steady grow of at least three predominant aromatic oxidation products of **5** was monitored by ^{1}H NMR spectra for a period of sixteen days (Fig. S3). An in-depth analysis of these reactions was not pursued because our main purpose here was to find handling and working conditions for the sulfides. As expected, the time dependent ^{1}H NMR analysis of anthracene sulfides showed that the oxidation reaction does not proceed if the air equilibrated solutions are kept in the dark. Therefore, the synthesis and the recrystallization steps of the anthracene sulfides were done in darkened glassware while purification by column chromatography was avoided. On the other hand, pyrene-based polysulfides dissolved in $CHCl_3$ or THF were fully stable in ambient conditions for weeks and no additional signals were found in their ^{1}H NMR spectra. It must be stressed, however, that all the polysulfides studied here, either

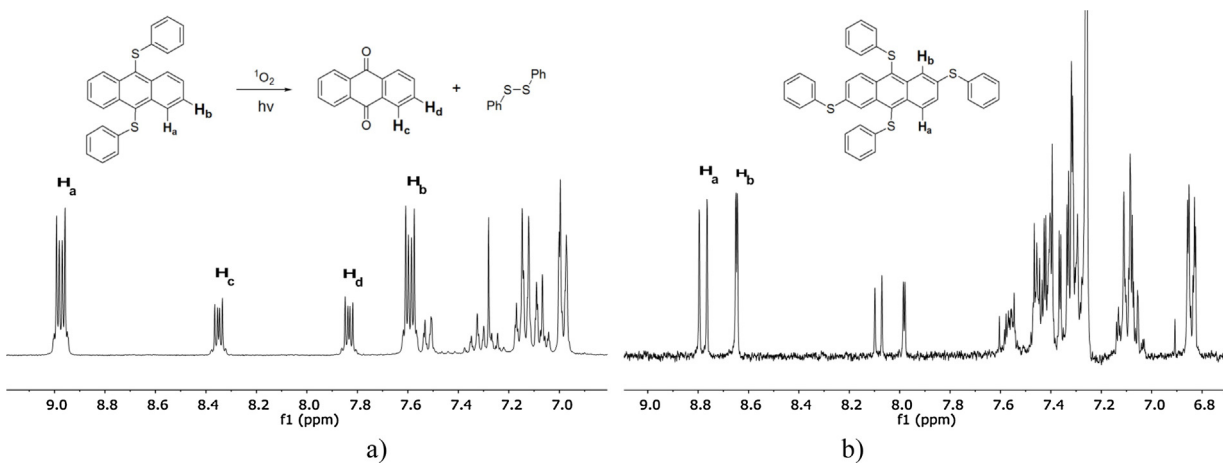

Fig. 1. Aromatic region of the ^{1}H NMR spectra. a) Solution of **1** in $CDCl_3$ kept for 3 days at ambient conditions (24 °C, fluorescent lighting). b) Mixture obtained after recrystallization of **2a** in toluene, kept for *ca.* 10 min at 110 °C, under air and ambient light.

anthracene- or pyrene-based, are stable for weeks if solutions are kept in the dark or for prolonged periods of time in solid state.

3.3. Photophysical properties

The photophysical data of the sulfides in THF solution, along with data of anthracene, **A**, and pyrene, **P**, included for comparison purposes, is reported in Table 1 while the absorption and emission spectra are shown in Figs. 2 and 3. The luminescence of sulfides was studied in both aerated and deaerated THF solutions. The profiles of the emission spectra obtained in the presence and absence of dioxygen were similar. It is relevant to note that the anthracene core presents all optical signatures of rigid chromophores having $S_0 \rightarrow S_1$ transitions with slight geometry differences between planar S_0 and S_1 states (Fig. S4), that is, a very small Stokes shift, SS, of 209 cm^{-1}, strong vibronic coupling and mirror image symmetry [38]. In the anthracene sulfides **1**, **2**, **3** and **4** (Fig. 2a and b), the absorption spectra partially retain the vibronic splitting of **A** indicating either a small distribution of ground-state geometries or that the rotamers generated by the substituent groups do not bear upon the electronic properties of the central rigid core. However, the mirror image symmetry is lost. Increasing bathochromic shifts of the absorption λ_{max} are observed with increasing number of phenylthio substituents, e.g., **A** (377 nm), bis(phenylthio) **1** (416 nm) and tetrakis(phenylthio) **2** (448 nm). Thus, the 9,10-disubstitution produces a red shift of 0.31 eV and then the additional 2,6-disubstitution further increases the red shift by 0.2 eV. Clearly, the sulfur atoms became integrated into the chromophoric core and a larger effect of the 9,10- than the 2,6-substitution is expected considering that the dipole moment of the $S_0 \rightarrow S_1$ transition corresponds to a transition dipole moment along the short anthracene axis (Fig. S4). The substitution of an *ortho*-hydrogen atom for a chlorine atom in the phenyl rings of **2** increases the absorption cross section of **3** but leaves its absorption λ_{max} almost unaltered, thus indicating that little interaction occurs between the polysulfurated central aromatic core and the aryl substituents. Likewise, only small changes in the absorption spectra are observed when the aryl groups are replaced by their alkyl counterparts, namely, between **2** and **4** (Fig. 2b) or between **5** and **6** (Fig. 2c). The molar extinction coefficients, ε, showed small variations and lay in a range of ± 30% of the value of **A**, with the exception of the above mentioned case of **3**.

The emission bands of the sulfides are devoid of vibronic structure, show moderate Stokes shifts and are markedly red-shifted compared to that of anthracene. Thus, the increase of thioether groups in the anthracene core produces a red shift from 380 nm (**A**) to 458 nm in the disulfide (**1**) and then to ~480 nm in all the anthracene tetrasulfides. The bis(phenylthio) **1** shows a large SS (2204 cm^{-1}) and very low quantum yield, $\Phi_F = 0.02$ either in air equilibrated or deaerated THF solutions, that is, a value close to that reported for **1** in air-equilibrated $CHCl_3$ solution ($\Phi_F = 0.038$) [18]. In order to be certain that the low yields were due to an intrinsic nonradiative path, measurements were done in deaerated THF solutions and immediately after the solutions were prepared and kept in darkened vials to avoid the presence of even minute quantities of the photooxidation products. On the contrary, smaller SS and augmented QY were observed with the additional 2,6-substitution. Thus, the tetrasulfides **2**, **3** and **4** have Stokes shifts of ~ 1550 cm^{-1} and Φ_F in the range of 0.24-0.49 in air equilibrated solutions and 0.26–0.59 in aerated solutions, with the highest efficiencies corresponding to the tetraalkyl sulfide **4**.

The substitution of sulfur by oxygen at the 2,6-positions of anthracene produces a small hypsochromic shift in the absorption spectra, that is, the λ_{max} is displaced from 448 nm in **2** to 440 nm in **5**. Similarly, a blue shift of nearly 10 nm is observed when going from **4** to **6** (Fig. 2c). Therefore, chalcogen variation from S to O at the 2,6-positions have a minor effect on the λ_{max} of the lowest energy absorption transitions and parallels equal chalcogen substitution at the 9,10-positions of the anthracene ring, e.g., the 409 nm absorption maxima of 9,10-bis(methylthio) anthracene shifts slightly to 404 nm in 9,10-dimethoxyanthracene [39]. Interestingly, despite the presence of the 9,10-disulfide substituents, both **5** and **6** closely resemble the characteristic absorption spectra of 2,6-dialkoxyanthracenes which present two well defined absorption bands at 403 nm and 339 nm [40]. Thus, two vibronically structured electronic transitions with origin at 448 nm and 360 nm can be observed in the absorption spectrum of **6** which are somewhat less defined in **5**. The fluorescence of mixed 2,6-dialkoxy-9,10-disulfides **5** and **6** have moderately blue shifted λ_{max} and slightly larger Stokes shift (~1900 cm^{-1}) and higher quantum efficiencies compared to the tetrasulfides. Again, the QY near unity in the absence of oxygen of **6** resembles the one presented by 2,6-dialkoxyanthracene.

The pyrene tetrasulfides are yellow powders except the disulfide **1P** which has a whitish appearance. As in anthracene, the ground state and the first relaxed state of pyrene are planar [41] but its apparently large SS of 2951 cm^{-1} arises because the strong absorption at 336 nm corresponds to the high energy bright $S_0 \rightarrow S_2$ transition while emission is originated by the $S_0 \rightarrow S_1$ transition. The lowest energy dark $S_0 \rightarrow S_1$ transition, which has been observed in gas phase at *ca.* 367 nm, [42] is very weak and not usually observed in standard absorption measurements in solution (Fig. S4). So, even though the anthracene and pyrene cores absorb in rather different wavelengths they both emit in the same region, yet **P** exhibits larger ε_{max} and Φ_F than **A**. In contrast to **P**, as a result of the influence of the substituents in 1, 3, 6 and 8 positions in both

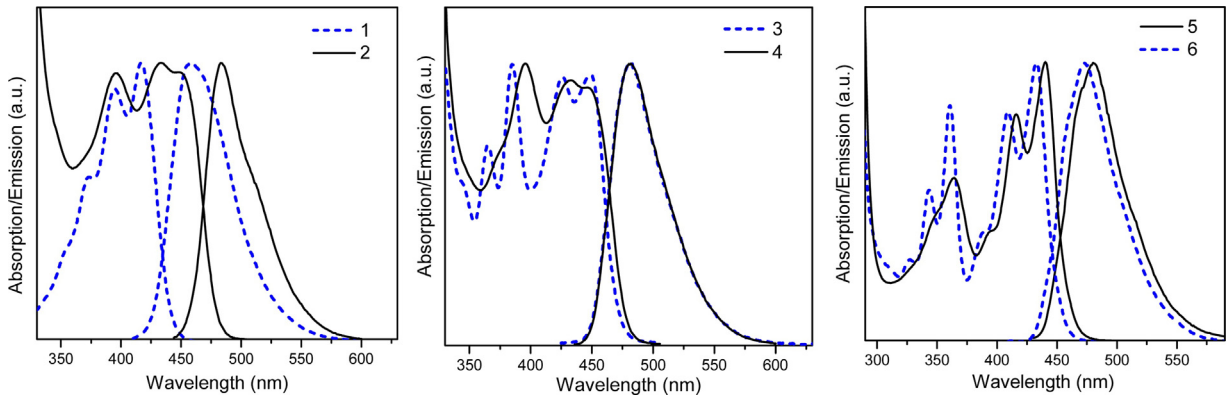

Fig. 2. Normalized absorption and emission spectra of THF solutions of the anthracene sulfides.

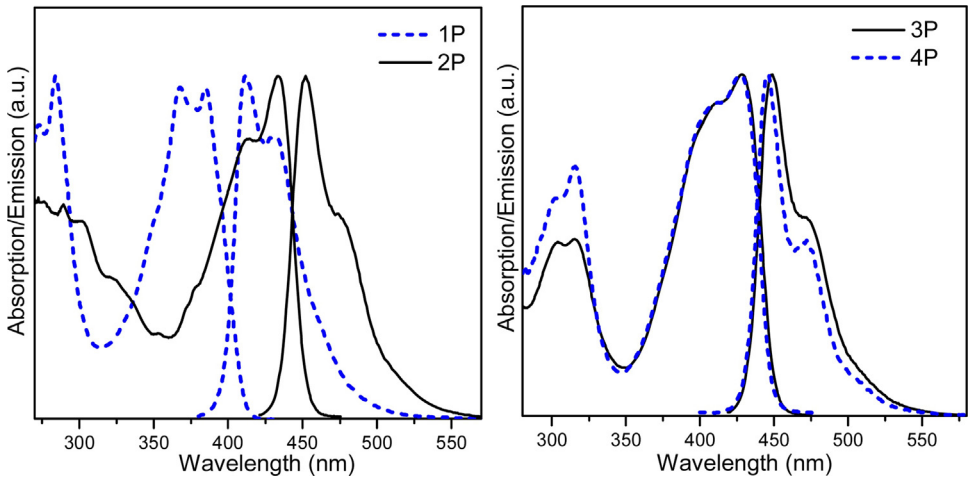

Fig. 3. Normalized absorption and emission spectra of THF solutions of the pyrene sulfides **1P-4P**.

$S_0 \rightarrow S_1$ and $S_0 \rightarrow S_2$ excitations, the low energy absorption transitions of the pyrene sulfides extend into the visible, are strongly allowed, showed a significant overlap with their fluorescence bands and bear some mirror-image relationship to the emission spectra.

A comparison with the reported λ_{max} of 367 nm of the dark $S_0 \rightarrow S_1$ transition of **P** indicated that, as the number of phenylthio substituents in the pyrene ring increased, the bathochromic shifts of the λ_{max} increased (Fig. 3a). Likewise, the emission maximum shifts from 373 nm (**P**) to 412 nm (**1P**) and to ~450 nm (**2P**, **3P** and **4P**). Replacement of the pendant aryl moiety of **2P** by R-CH_2- groups produces a very small blue shift (~5 nm) in both the absorption and the emission spectra of benzylsulfide **3P** as well as in dodecylsulfide **4P**. Both sulfides **3P** and **4P** have nearly equivalent bands (Fig. 3b) thus indicating that insertion of a single sp^2 carbon suffices to break whatever small conjugation is occurring through the sulfur atom between the pyrene and phenyl groups. Therefore, the similar influence of the substituents on the absorption and emission bands, the small Stokes shift and high extinction coefficients indicate that the lowest energy absorption bands could correspond to the overlap of a now bright lower energy $S_0 \rightarrow S_1$ transition and a higher energy $S_0 \rightarrow S_2$ transition which are both bathochromically shifted as has been observed in 1-substituted pyrenes [43]. Analogous to the anthracene sulfides, the pyrene sulfides here studied showed smaller Stokes shifts with increased substitution. However, quantum yields are influenced by the nature of the pendant groups instead of its number. Thus, arylsulfides **1P** and **2P** showed Φ_{em} values *ca.* 0.3 while alkylsulfides **3P** and **4P** exhibit larger Φ_{em} values in the range of 0.7-0.9 in deaerated solutions.

The absorption and emission spectra of **1**, **2**, **5**, **1P** and **2P** were measured in other solvents of variable polarity (EtOH, CH_3CN and CCl_4) to observe any potential solvatochromic effects (Table 2). The shifts of the maxima with respect to the one observed in CCl_4 are below 5 nm; with the exception of the one observed for the emission of **1** in acetonitrile. So, no considerable variations in the λ_{max} or in the λ_{em} were observed as the solvent polarity increases suggesting that these transitions do not imply significant reorganization of the molecular electronic density upon excitation. All sulfides were soluble in non-polar solvents (CCl_4 and THF) but solubilities decreased markedly in acetonitrile and even more in ethanol. Excimer formation is often an undesired property when the potential applications of electron rich aromatic chromophores are considered. However, for these series of sulfides, solutions in CCl_4 or THF did not show additional emission bands which would indicate excimer formation even at concentrations as high as 5×10^{-3} M.

Table 2
Absorption and emission maxima in various solvents.

Solvent		1		2		5		1P		2P	
	$E_T(30)$[a]	λ_{max}	λ_{em}	λ_{max}	λ_{em}	λ_{max}	λ_{em}	λ_{max}	λ_{em}	λ_{max}	λ_{em}
CCl_4	32.4	418	456	451	482	440	477	385	412	429	451
THF	37.4	416	458	448	483	440	480	384	412	435	453
CH_3CN	45.6	414	467	449	483	438	480	383	414	432	452
EtOH	51.9	413	456	451	480	437	477	384	409	432	447

[a] Dimroth-Reichardt polarity parameter.

3.4. Theoretical calculations

The geometries of the conformers up-down, *ud*, and up-up, *uu*, of **1** displayed in Fig. 3a and b were investigated at the B3LYP-D3/def2-TZVP(-f)/COSMO(THF) level of theory. The relative energies were found to be quite similar ($E_{ud} - E_{uu} = 0.02$ Kcal mol^{-1}). This suggests that both conformers contribute almost equally to the absorption spectra. Moreover, the values of the vertical absorptions of both conformers calculated at the TDDFT/BHLYP level are also alike, $\lambda^{vert-a}(ud) = 358$ nm and $\lambda^{vert-a}(uu) = 359$ nm. Similar results have been obtained for multiarmed aryl ethers carrying from two to eight arylmethylene side-chains in a variety of aromatic cores, that is, the computed UV–vis spectra of several conformers were essentially the same [44].

Therefore, only a selected structure with opposite groups in their up and down conformations was considered for each arylsulfide in the following simulations, e.g. the *udud* conformation of **2**, see Fig. 3c. The flexible side chains were replaced by methyl groups in order to scale down the computational expenses. The computed geometry of the sulfides have the methyl groups of the 2,6-dialkoxy and 2,6-disulfide groups situated in the plane of the central core while the methyl groups in the 9,10-anthacenyl sulfide groups adopt up and down conformations.

The one-electron picture of an excited state is a simple model where the excitation of an electron is visualized as occurring from an occupied to a virtual molecular orbital. So, in order to discuss structure-properties relationships, it is customary to correlate the experimental optical band-gaps measured from the absorption spectra, E_g^{opt}, with the difference in energy between frontier molecular orbitals (FMO), E_{LUMO}-E_{HOMO}, obtained by the geometry optimization process. The E_g^{opt} of the polysulfides determined from the onset of the energetically lowest absorption band along with HOMO-LUMO gaps computed with the DFT/B3LYP-D3/

Table 3
Comparison of experimental and calculated excitation energies (in eV).

Cpds	Exptl[a]	DFT band-gap[b]			Exptl[c]	TD-DFT[d]			
	Eg^{opt}	E_{HO}	E_{LU}	E_{LU}-E_{HO}	λ_{max}	λ^{vert-a}	State	f^{e}	Configuration[f]
A	3.24	−5.49	−1.92	3.57	3.29	3.77	1	0.109	H → L 92
						5.94	5	0.523	H − 1 → L 48
									H → L + 1 47
1	2.82	−5.76	−2.45	3.30	2.97	3.48	1	0.285	H → L 92
2	2.59	−5.64	−2.55	3.09	2.75	3.34	1	0.334	H → L 91
						3.59	2	0.115	H − 1 → L 91
3	2.58	−5.56	−2.54	3.04	2.77	3.22	1	0.170	H → L 93
4[g]	2.63	−5.25	−2.28	2.97	2.77	3.22	1	0.209	H → L 93
						3.88	2	0.036	H − 1 → L 57
									H → L + 1 36
5[g]	2.64	−5.34	−2.16	3.18	2.82	3.35	1	0.248	H → L 93
						3.99	2	0.073	H − 1 → L 50
									H → L + 1 37
6[g]	2.72	−5.20	−2.08	3.12	2.86	3.47	1	0.916	H → L 91
						4.07	2	0.056	H − 1 → L 63
									H → L + 1 32
P	3.65	−5.59	−1.75	3.84	3.69	4.10	1	0.001	H → L + 1 55
						4.18	2	0.353	H − 1 → L 45
									H → L 80
									H − 1 → L + 1 18
1P	3.02	−5.69	−2.22	3.47	3.23	3.76	1	0.554	H → L 85
						4.18	4	0.112	H − 2 → L 69
2P	2.74	−5.38	−2.36	3.02	2.85	3.33	1	0.997	H → L 90
4P[g]	2.77	−4.86	−1.82	3.04	2.90	3.41	1	0.914	H → L 92

[a] Optical HOMO/LUMO gaps were defined by the onset wavelength of the longest wavelength absorption in THF solution, Eg^{opt} (eV) = 1240/λ_{max}^{onset} (nm).
[b] From optimized geometries at the DFT-B3LYP-D/TZVP(-f)/COSMO (THF) level.
[c] Experimental excitation energy for the maximal absorption of the lowest energy transition in THF solution.
[d] Vertical transitions energies calculated at the TD-DFT-BHLYP/TZVP(-f)//B3LYP-D/TZVP(-f)/COSMO (THF) level.
[e] Oscillator strengths of the first five states, only transitions with $f > 0.035$ are listed, except for **P**.
[f] Configuration (with contribution in%, only contributions of >10% are listed).
[g] The calculated values correspond to the methyl analogue of the polysulfide.

COSMO(THF) approach are listed in Table 3. The DFT band-gaps thus calculated are systematically 0.3–0.5 eV higher than experimental optical gaps. Interestingly, the calculations indicate that sulfur substitution affects both HOMO and LUMO levels in a similar pattern irrespective of the nature of the central aromatic core. Thus, both bis(phenyl sulfide)s **1** and **1P** present a decrease in the energy of their HOMO and LUMO levels, albeit the effect is stronger on the LUMO level, so these disulfides present a bathochromic shift with respect to their parent aromatic hydrocarbons (Fig. 4). The tetrakis(phenylsulfide)s **2** and **2P** show a red shift compared to their related bis(phenyl sulfide)s **1** and **1P** due to an increase in the HOMO energies and a decrease in the LUMO energies. The replacement of the aromatic moieties by alkyl chains produces an increase in the energy of both FMOs of **4** and **4P**, so the band gaps change only slightly. Therefore, the modeling matches the absorption behavior of the tetraalkyl and the tetraaryl derivatives, either anthracene-based or pyrene-based whose experimental E_g^{opt} showed minor variations. Apparently, this insensitiveness would be circumscribed to the band gap because computation results suggest that alkyl derivatives should be better donor and worse electron acceptors than the aryl ones. In addition, the calculations reproduced nicely the insensitiveness of the chlorine substitution in **3** and blue shifts observed in **5** and **6**. Thus, while the presence of a chlorine atom on the phenyl substituents in **3** practically does not bear on the frontier energy levels, the replacement of the sulfur by more electronegative oxygen atoms

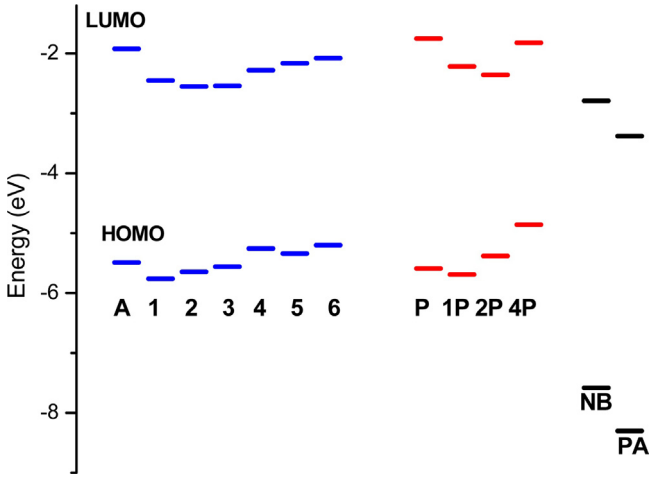

Fig. 4. Calculated FMO energies at the B3LYP-D3/def2-TZVP(-f)/COSMO(THF) level of anthracene and pyrene sulfide and the electro deficient compounds nitrobenzene (NB) and 2,4,6-trinitrotoluene (TNT).

in the 2,6 position of the anthracene derivative **3** widens the FMO gap.

A more elaborate picture of electronic excitations describes them in terms of multielectronic states where a given optical transition is represented by a linear combination of several occupied-to-virtual MO excitations. Time-dependent density functional theory (TD-DFT) permits nowadays the calculation of excited state properties of fairly large systems according to this approach [45]. Initially, TD-DFT calculations of the vertical absorptions, λ^{vert-a}, of the disulfides in THF were performed with the B3LYP functional but although absolute values of λ^{vert-a} are in the range of the experimental λ_{max}, they showed large dispersions. It was satisfactory to observe that results obtained with the hybrid BHLYP functional consistently followed the experimental trend, i.e., the linear relationship between λ_{max} and λ^{vert-a} showed a correlation coefficient of R = 0.987, although the experimental excitation energies were systematically underestimated by 0.5 eV ± 0.04 eV, see Table 3. So, we concluded that bathochromic shifts are well reproduced by theory and the BHLYP method would be useful in the design of novel polysulfurated arenes. Moreover, in the computationally difficult case of pyrene, the bright $S_0 \rightarrow S_2$ transition is correctly described with a dominant contribution of the HOMO → LUMO transition possessing a sizable oscillator strength, $f = 0.353$, and higher energy than the dark $S_0 \rightarrow S_1$ transition which has comparable contributions of the HOMO–1 → LUMO and HOMO → LUMO + 1 transitions and a very small f of 0.001 (Table 3). However, the modeling of hyperchromic/hypochromic shifts is less satisfactory and only predicts correctly that pyrene derivatives show higher absorptivity values than the anthracene sulfides($f_{P\text{-sulfides}} > f_{A\text{-sulfides}}$), but the differences between each family are on the whole not well reproduced.

The analysis of the lowest energy multielectronic states of the anthracene sulfides showed that the lower energy transitions can be mainly attributed (>90% contribution) to the HOMO → LUMO promotion which correspond to the $S_0 \rightarrow S_1$ transition along the short axis of anthracene which has a covalent character. So, a $\pi(core) \rightarrow \pi^*(core)$ character dominates these transitions that will show only marginal charge-transfer characteristics as it was evidenced by the quite small solvatochromic effect observed for the anthracene sulfides. Indeed, neither of states obtained by TD-DFT described the lower energy excitations as having two comparable contributions (HOMO → LUMO + 1 and HOMO–1 → LUMO) which would then present a mixed $n \rightarrow \pi^*(core)/\pi(phenyl) \rightarrow \pi^*(core)$ nature with significant charge transfer characteristics. These mixed transitions occurred as high energy states in anthracene and the anthracene sulfides **4**, **5** and **6**. Similarly, the TD-DFT calculations of pyrene sulfides described the lowest energy absorption as a strongly allowed HOMO → LUMO transition. So, our DT-DFT calculations indicate that the lower energy excitations in both anthracene and pyrene sulfides are of non-ionic type in agreement with experimental results which showed both absorption and emission spectra devoid of noticeable solvatochromic effects.

The analysis of the topologies of the frontier orbitals (Fig. 5) confirms the above observations. It can be observed that the related tetrasulfides **2** and **2P** have very similar electron distribution patterns. That is, their LUMOs are delocalized mostly over the central aromatic core while the HOMOs are also extended

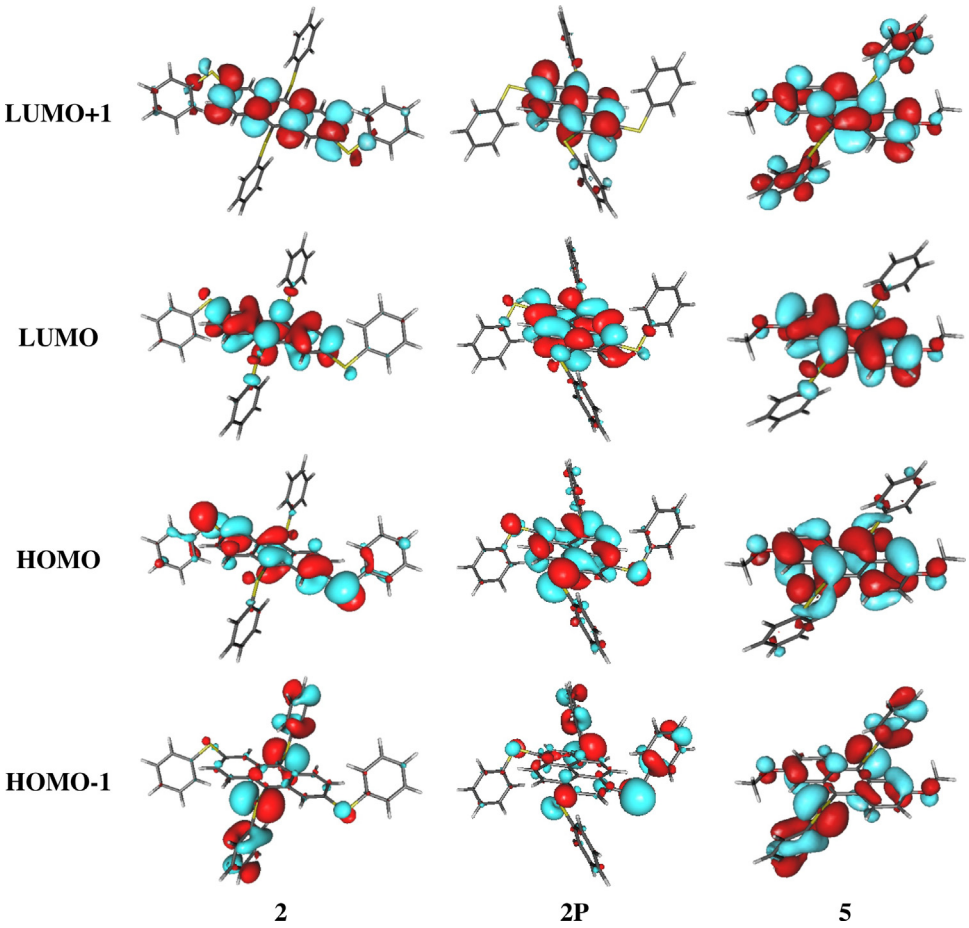

Fig. 5. Frontier orbitals of sulfides. Figure uses a isocontour of value 0.025 a.u.; for color figure the reader is referred to the web version of this article.

to the sulfur atoms, though only two of them contribute significantly to the orbital. Thus, the sulfur atoms attached to the 9,10 positions of **2** are weakly integrated to the HOMO while in **2P**, due to the symmetric nature of the chromophore, the HOMO have a notable contribution from two sulfur atoms situated in opposite positions, e.g.: 1 and 6, while the other two, e.g.: 3 and 8, have reduced contributions. On the contrary, in sulfide **5** the contribution of the 9,10-sulfur atoms to the HOMO is higher than that of the 2,6-oxygen atoms. In all cases the HOMO-LUMO transitions encircling only the aromatic cores and some of the heteroatoms indicate that no significant electronic reorganizations are expected upon excitation. Since the alkyl and aryl substituents do not contribute to the orbitals involved in the transition, their effect is limited to the processing and thermal properties of the sulfides as well as on their fluorescence efficiencies

3.5. Interaction with electron deficient nitroaromatic compounds

We then studied the interaction of the electron rich anthracene sulfides with the electron deficient nitroaromatic compounds, NACs, whose detection is of interest for environmental and security reasons [25,46]. Nitrobenzene, NB, and 2,4,6-trinitrotoluene, TNT, were chosen among the nitroaromatic compounds as quenchers because they show minimal quenching by resonance energy transfer and inner filter effects even at concentrations as high as 10^{-3} M because their absorption maxima lie in regions (>300 nm) far from the $\lambda_{exc} \sim 400$ nm used in the quenching experiments or the emission region of the sulfides (400–500 nm). The remaining quenching process, i.e., electron transfer from the excited state of the sulfide to the ground state of TNT [46], requires close encounter of the sulfide with the analyte, thus its quenching efficiency depends on both electronic and steric factors. The analysis of the DFT calculations indicates that electronic factors are favorable for both quenchers. Thus, examination of the HOMO-LUMO energy levels shows that the LUMOs of the NB and TNT rest below the LUMOs of the anthracene and pyrene sulfides thus providing the necessary driving force for the oxidative electron transfer (Fig. 4). Steric effects are more difficult to evaluate a priori though for application purposes it is expected that the groups attached to the periphery of the aromatic central core present steric hindrances large enough to impede the aggregation-caused self-quenching but not the interaction with analytes [47].

Thus, we carried out fluorescence quenching screening experiments by measuring the fluorescence intensity responses, $(I_0\text{-}I/I_0)$ x100, of the sulfides upon the addition of the quencher to explore the ability of the anthracene and pyrene tetrasulfides to interact with nitroaromatic compounds. Control experiments in the absence of the quencher indicated that the anthracene sulfides did not show a reduction of fluorescence intensities due to photobleaching during the course of the quenching observations. The fluorescence intensity of phenyl substituted sulfides **2**, **3** and **2P** did not diminish upon the addition of TNT, Fig. 6a. However, the partial or total substitution of the bulkier phenyl groups linked to the sulfur by smaller methylene groups resulted in a moderate decrease in the fluorescence intensity of **4**, **5**, **6**, **3P** and **4P**. Subsequent experiments showed that all sulfides were more sensitive to NB than to TNT. In fluorescence quenching titration experiments with **6**, the gradual addition of either TNT or NB caused a steady decrease of the fluorescence intensities (Fig. 6b). The Stern-Volmer analysis of fluorescence quenching titration experiments of **6** afforded linear relationships with R^2 values of >0.99 with Stern-Volmer constants (K_{SV}) of 118 M^{-1} for NB and 56 M^{-1} for TNT. These K_{SV} values are smaller than those presented by pyrene with NB (K_{SV} = 315 M^{-1}) [48], thus indicating that steric hindrance is dominant in defining the quenching ability of these anthracene and pyrene sulfides in processes that require a close molecular encounter.

4. Conclusions

A series of disulfides and tetrasulfides with anthracene or pyrene central cores with aryl and alkyl pendant groups were obtained by nucleophilic aromatic substitution. All sulfides are crystalline compounds and show good chemical stability in condensed phase. In solution, the pyrene derivatives are very stable but the anthracene derivatives suffer a slow photooxidation process under air and ambient light.

Increasing bathochromic shifts of the absorption and emission bands were observed with increasing number of phenylthio or alkoxy substituents in the anthracene indicating that the sulfur and oxygen atoms became integrated into the chromophoric core. The structural modification of the pendant groups leave absorption and emission bands almost unaltered, indicating that little interaction occurs between the central aromatic core and the alkyl or aryl substituents. However, quantum yields are influenced by the nature of the pendant groups. All tetrasubstituted anthracene sulfides are highly fluorescent with good quantum yields. In particular, the mixed 2,6-dialkoxy-9,10-disulfides present large quantum efficiencies close to unity.

While the bisulfides of anthracene and pyrene have very different spectroscopic behavior, the tetrasubstituted anthracene and pyrene sulfides exhibit quite a few similarities. Thus, the

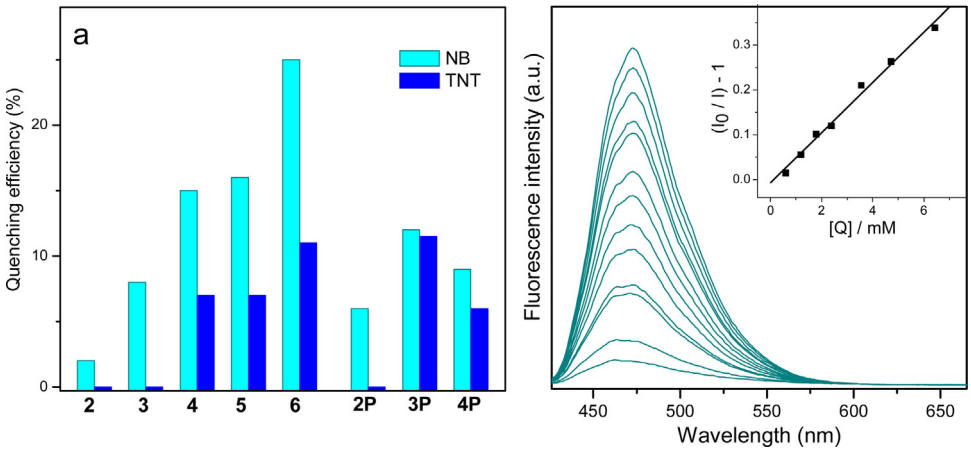

Fig. 6. a) Fluorescence intensity responses of sulfides in THF solution upon the addition of NB or TNT in THF; [Sulfide] = 3 μM, [Q] = 2.4 mM. b). Steady-state fluorescence quenching of **6** in THF solution (3.0 μM) with TNT (0.15 m M–1.1 m M; top to bottom); excited at 405 nm in the right angle geometry. Inset refer to Stern-Volmer plot.

chromophoric core of the compounds consists of the aromatic core and the sulfur or oxygen atoms, so the variation from alkyl to aryl substituents does not alter the profiles of the absorption and emission spectra. All show intense fluorescence, but sulfides bearing SCH_2 or OCH_2 groups display higher fluorescence efficiencies than the ones with aryl substituents. In addition, due to the presence of the substituent groups they do not form excimers and their quenching efficiencies of both series is dominated by steric hindrance rather than by electronic factors.

The calculated HO-LU gaps (DFT-B3LYP) broadly described the optical gap trends while the TD-DFT-BHLYP calculations of the vertical absorptions consistently followed the experimental trend suggesting that the BHLYP method would be useful in the design of novel polysulfurated arenes. The analysis of the multielectronic states indicated that the lower energy transitions can be attributed to the HOMO → LUMO promotion while the topologies of the frontier orbitals indicated that a non-ionic $\pi(core) \rightarrow \pi^*(core)$ character dominate these excitations in agreement with experimental results which showed both absorption and emission spectra devoid of noticeable solvatochromic effects.

Acknowledgments

Financial support from SGCyT-UNS and CIC-PBA is acknowledged. CMH and MJR thank CONICET for a fellowship. PGDR and ROG are members of the research staff of CONICET.

Appendix A. Supplementary data

Supplementary data associated with this article can be found, in the online version, at http://dx.doi.org/10.1016/j.jphotochem.2017.07.011.

References

[1] H.R. Kricheldorf, O. Nuyken, G. Swift, Handbook of Polymer Synthesis, 2nd ed., Marcel Dekker, New York, 2005.
[2] J. Vicente, J.A. Abad, R.M. Lopez-Nicolas, Synthesis of molecular chains: phenylene thioether and sulfoxide oligomers, Tetrahedron 64 (2008) 6281–6288.
[3] O. Goyot, M. Gingras, p-Phenylene sulfide oligomers and their properties. A-S couplings mediated by copper or by fluorine substitutions, Tetrahedron Lett. 50 (2009) 1977–1981.
[4] S. Kumar, Self-organization of disk-like molecules: chemical aspects, Chem. Soc. Rev. 35 (2006) 83–109.
[5] A.N. Cammidge, H. Gopee, Structural factors controlling the transition between columnar hexagonal and helical mesophase in triphenylene liquid crystals, J. Mater. Chem. 11 (2001) 773–783.
[6] M. Gingras, J.M. Raimundo, Y.M. Chabre, Persulfurated aromatic compounds, Angew. Chem. Int. Ed. 45 (2006) 1686–1712.
[7] M. Gingras, V. Placide, J.M. Raimundo, G. Bergamini, P. Ceroni, V. Balzani, Polysulfurated pyrene-cored dendrimers: luminescent and electrochromic properties, Chem. Eur. J. 14 (2008) 10357–10363.
[8] T.D.P. Stack, R.H. Holm, Subsite-differentiated analogs of biological [4Fe-4S] 2+ clusters: synthesis, solution and solid-state structures, and subsite-specific reactions, J. Am. Chem. Soc. 110 (1988) 2484–2494.
[9] D. Atilla, N. Kilinç, F. Yuksel, A.G. Gürek, Z.Z. Öztürk, V. Ahsen, Synthesis, characterization, mesomorphic and electrical properties of tetrakis(alkylthio)-substituted lutetium(III) bisphthalocyanines, Synth. Met. 159 (2009) 13–21.
[10] G. Heywang, L. Born, S. Roth, New radical cation salts of substituted pyrenes, Synth. Met. 41 (1991) 1073–1078.
[11] G. Heywang, L. Born, S. Roth, Radical cation salts of 1, 3, 6, 8-tetrakis (methylthio)-pyrene-new easily accessible compounds with high electrical conductivity and excellent stability, Angew. Chem. Int. Ed. 30 (1991) 176–177.
[12] M. Gingras, A. Pinchart, C. Dallaire, T. Mallah, E. Levillain, Star-shaped nanomolecules based on p-phenylene sulfide asterisks with a persulfurated coronene core, Chem. Eur. J. 10 (2004) 2895–2904.
[13] A. Kimoto, K. Tanaka, M. Kawahata, K. Yamaguchi, S. Otsubo, Y. Sakai, Y. Ono, A. Ohno, K. Kobayashi, Bis(methylthio)tetracenes: synthesis, crystal-packing structures, and OFET properties, J. Org. Chem. 76 (2011) 5018–5025.
[14] A. Fermi, G. Bergamini, R. Peresutti, E. Marchi, M. Roy, P. Ceroni, M. Gingras, Molecular asterisks with a persulfurated benzene core are among the strongest organic phosphorescent emitters in the solid state, Dyes Pigm. 110 (2014) 113–122.
[15] A. Fermi, G. Bergamini, M. Roy, M. Gingras, P. Ceroni, Turn-on phosphorescence by metal coordination to a multivalent terpyridine ligand: a new paradigm for luminescent sensors, JACS 136 (2014) 6395–6400.
[16] K.K. Baldridge, K.I. Hardcastle, T.J. Seiders, J.S. Siegel, Synthesis, structure and properties of decakis(phenylthio)corannulene, Org. Biomol. Chem. 8 (2010) 53–55.
[17] A. Fermi, P. Ceroni, M. Roy, M. Gingras, G. Bergamini, Synthesis, characterization, and metal ion coordination of a multichromophoric highly luminescent polysulfurated pyrene, Chem. Eur. J. 20 (2014) (10840-10840).
[18] C. Nerungsi, P. Wanitchang, S. Sahasithiwat, K. Sadorn, T. Kerdcharoen, T. Thongpanchang, Organic electroluminescence devices based on anthracene sulfide derivatives, Tetrahedron Lett. 51 (2010) 6392–6395.
[19] T. Brotin, J.-P. Desvergne, F. Fages, R. Utermöhlen, R. Bonneau, H. Bouas-Laurent, Photostationary fluorescence emission and time resolved spectroscopy of symmetrically disubstituted anthracenes on the meso and side rings: the unusual behavior of the 1, 4 derivative, Photochem. Photobiol. 55 (1992) 349–358.
[20] W. Sotoyama, H. Sato, A. Matsuura, N. Sawatari, Ab initio configuration interaction singles (CIS) study on polycyclic aromatic molecules (II): predicting fluorescence quantum yields by calculating the excitation energies, J. Molec. Struct.: Theochem. 9 (756) (2005) 35–38.
[21] E. Hasegawa, S. Takizawa, T. Seida, A. Yamaguchi, N. Yamaguchi, N. Chiba, T. Takahashi, H. Ikeda, K. Akiyama, Photoinduced electron-transfer systems consisting of electron-donating pyrenes or anthracenes and benzimidazolines for reductive transformation of carbonyl compounds, Tetrahedron 62 (2006) 6581–6588.
[22] A. Dadvand, W.H. Sun, A.G. Moiseev, F. Bélanger-Gariépy, F. Rosei, H. Meng, D.F. Perepichka, 1, 5-, 2, 6-and 9, 10-distyrylanthracenes as luminescent organic semiconductors, J. Mater. Chem. C 1 (2013) 2817–2825.
[23] M. Sun, D. Zhang, Y. Li, J. Wang, Y. Gao, W. Yang, Aggregation-enhanced emission and piezochromic luminescence of 9, 10-bis (p-dibutylaminostyryl)-2, 6-bis (p-t-butylstyryl) anthracene, J. Lumin. 148 (2014) 55–59.
[24] P.G. Del Rosso, M.J. Romagnolli, M.F. Almassio, C.A. Barbero, R.O. Garay, Diphenylanthrylene and diphenylfluorene-based segmented conjugated polymer films as fluorescent chemosensors for nitroaromatics in aqueous solution, Sens. Actuators B: Chem. 203 (2014) 612–620.
[25] P.G. Del Rosso, M.F. Almassio, M. Bruno, R.O. Garay, Mild persubstitution of di- and tetrabrominated arenes with arylthiolate nucleophiles, Tetrahedron Lett. 51 (2010) 6730–6733.
[26] F. Neese, The ORCA program system, Wiley Interdiscip. Rev. Mol. Sci. 2 (2012) 73–78.
[27] A.R. Allouche, Gabedit- a graphical user interface for computational chemistry softwares, J. Comput. Chem. 32 (2011) 174–182.
[28] S. Fratiloiu, F.C. Grozema, Y. Koizumi, S. Seki, A. Saeki, S. Tagawa, S.P. Dudek, L.D. A. Siebbeles, Electronic structure and optical properties of charged oligofluorenes studied by vis/nir spectroscopy and time-dependent density functional theory, J. Phys. Chem. B 110 (2006) 5984–5993 (A).
[29] J.A. Degheili, R.M. Moustafa, D. Patra, B.R. Kaafarani, Effect of chain length on the photophysical properties of pyrene-based molecules substituted with extended chains, J. Phys. Chem. A 113 (2009) 1244–1249.
[30] F. Weigend, R. Ahlrichs, Balanced basis sets of split valence, triple zeta valence and quadruple zeta valence quality for H to Rn: design and assessment of accuracy, Phys. Chem. Chem. Phys. 7 (2005) 3297–3305.
[31] A. Klamt, Conductor-like screening model for real solvents: a new approach to the quantitative calculation of solvation phenomena, J. Phys. Chem. 99 (1995) 2224–2235.
[32] A. Klamt, V. Jones, Treatment of the outlying charge in continuum solvation models, J. Chem. Phys. 105 (1996) 9972–9981.
[33] S. Grimme, Semiempirical GGA-type density functional constructed with a long-range dispersion correction, J. Comput. Chem. 27 (2006) 1787–1799.
[34] S. Hirata, Head-Gordon M. time-dependent density functional theory within the Tamm-Dancoff approximation, Chem. Phys. Lett. 314 (1999) 291–299.
[35] F. Neese, An improvement of the resolution of the identity approximation for the calculation of the coulomb matrix, J. Comp. Chem. 24 (2003) 1740–1747.
[36] F. Weigend, Accurate coulomb-fitting basis sets for H to Rn: design and assessment of accuracy, Phys. Chem. Chem. Phys. 8 (2006) 1057–1065.
[37] I. Kaur, W. Jia, R.P. Kopreski, S. Selvarasah, M.R. Dokmeci, C. Pramanik, N.E. McGruer, G.P. Miller, Substituent effects in pentacenes: gaining control over HOMO-LUMO gaps and photooxidative resistances, J. Am. Chem. Soc. 130 (2008) 16274–16286.
[38] M. Baba, M. Saitoh, K. Taguma, K. Shinohara, K. Yoshida, Y. Semba, S. Kasahara, N. Nakayama, H. Goto, T. Ishimoto, U. Nagashima, Structure and excited-state dynamics of anthracene: ultrahigh-resolution spectroscopy and theoretical calculation, J. Chem. Phys. 130 (2009) 134315.
[39] K. Kobayashi, H. Masu, A. Shuto, K. Yamaguchi, Control of face-to-face π-π stacked packing arrangement of anthracene rings via chalcogen–chalcogen interaction: 9, 10-bis(methylchalcogeno)anthracenes, Chem. Mater. 17 (2005) 6666–6673.
[40] X. Zhou, G.B. Piland, D. Kurunthu, R.J. Dillon, J.J. Burdett, C.J. Bardeen, The photophysics of the 2, 6-dialkoxy anthracenes: evidence for excited state side-chain conformational relaxation, J. Lumin. 132 (2012) 2997–3003.
[41] M. Baba, M. Saitoh, Y. Kowaka, K. Taguma, K. Yoshida, Y. Semba, S. Kasahara, T. Yamanaka, Y. Ohshima, Y.C. Hsu, S.H. Lin, Vibrational and rotational structure and excited-state dynamics of pyrene, J. Chem. Phys. 131 (2009) 224318.
[42] E.A. Mangle, M.R. Topp, Excited-state dynamics of jet-cooled pyrene and some molecular complexes, J. Chem. Phys. 90 (1986) 802–807.

[43] P. Trojanowski, J. Plötner, C. Grünewald, F.F. Graupner, C. Slavov, A.J. Reuss, M. Braun, J.W. Engels, J. Wachtveitl, Photo-physical properties of 2-(1-ethynylpyrene)-adenosine: influence of hydrogen bonding on excited state properties, Phys. Chem. Chem. Phys. 16 (2014) 13875–13888.
[44] T. Mori, S. Grimme, Y. Inoue, A combined experimental and theoretical study on the conformation of multiarmed chiral aryl ethers, J. Org. Chem. 72 (2007) 6998–7010.
[45] A.D. Laurent, D. Jacquemin, TD-DFT benchmarks: a review, Int. J. Quantum Chem. 113 (2013) 2019–2039.
[46] X. Sun, Y. Wang, Y. Lei, Fluorescence based explosive detection: from mechanisms to sensory materials, Chem. Soc. Rev. 44 (2015) 8019–8061.
[47] S. Shanmugaraju, S.A. Joshi, P.S. Mukherjee, Fluorescence and visual sensing of nitroaromatic explosives using electron rich discrete fluorophores, J. Mater. Chem. 21 (2011) 9130–9138.
[48] M.S. Meaney, V.L. McGuffin, Investigation of common fluorophores for the detection of nitrated explosives by fluorescence quenching, Anal. Chim. Acta 610 (2008) 57–67.